

## ATTRIBUTES OF DYNAMICAL EVENTS TO TROPOSPHERIC OZONE DISTRIBUTION OVER EQUATORIAL AFRICA

K. TURE & G. MENGISTU TSIDU

Department of Physics, Addis Ababa University, Ethiopia.

### ABSTRACT

Volcanic activity, biological decay, forest fires, thunderstorm events and stratospheric intrusions are key sources that introduce atmospheric traces to the troposphere. Ozone is one of such traces which can be found in very high concentration than its normal level due to natural factors. Upper and middle tropospheric ozone act as a green house gas while ozone found in high concentration at lower troposphere is a pollutant that harms living organisms. In few ozone and relative humidity data records by measurements of ozone by airbus in service aircraft (MOZAIC), spikes were observed at a flying altitude of 250–200 hPa at equatorial Africa. Equatorial Africa is one of the three thunderstorm hot spot regions (South America, Equatorial Africa and Southeast Asia) of the world. This work discusses how ozone of stratospheric origin produced enhanced ozone over the troposphere of equatorial Africa and its redistribution due to dynamical events. To understand the events that attribute to spiky MOZAIC ozone and relative humidity observations, in addition to MOZAIC ozone and relative humidity, data sets from different sources were used for diagnosis. Meridional cross-section of potential vorticity over the region of interest showed high potential vorticity (PV) intrusion below the tropopause level that induced enhanced ozone into upper troposphere. Vertical wind fields in the regions of low outgoing long wave radiation (OLR), very high latent heat and cloud liquid water content transport have indicated presence of convection and thunderstorm events. Enhanced ozone of stratospheric origin, as revealed by GOME satellite data produced during stratospheric intrusion, transported from the stratosphere all the way down to the boundary layer. Convective erosion was found to scavenge ozone concentration mainly at the boundary layers between 1000 and 700 hPa and enhanced ozone volume mixing ratio (VMR) of 60–100 ppbv which exceeds the WHO guideline limit of 60 ppbv were observed. These events have led to ozone pollution.

*Keywords: convection, latent heat, OLR, ozone spikes, pollution, PV-intrusion, scavenging, thunderstorm, wind fields.*

### 1 INTRODUCTION

Ozone in the atmosphere exerts different influence on the well being of man. Stratospheric ozone, where approximately 90% of the atmospheric ozone is found, produced mainly by photochemical reaction, prevents the sun's ultraviolet (UV) radiation reaching the surface of the earth. In the troposphere, ozone is photo-chemically produced through a combination of chemical reactions involving a variety of volatile organic compounds (VOCs) and nitrogen oxides (NO<sub>x</sub>), which are emitted by motor vehicles, by large stationary sources and by natural sources [1]. Middle and upper troposphere ozone is direct green house gas while in the boundary layer, it is a pollutant, which has harmful effect on human, animal and crops.

Tropical ozone controls atmospheric chemical composition and affects global climate and air quality through large scale redistribution. Over the tropics, Africa is an important reservoir of ozone precursor sources allowing ozone to build up through active photochemistry exacerbated by high solar radiations. The most important sources of ozone precursors over equatorial Africa are biomass burning [2], biogenic [3] and lightning [4]. These sources present a strong regional seasonality. In particular, biomass burning products have substantial influence on O<sub>3</sub> mixing ratios [5]. These emissions account for half of the global carbon monoxide (CO) emissions [6]. Furthermore according to Marufu *et al.* [2], pyrogenic emissions account for 16% of the ozone burden over Africa through different land type burning (mostly savannas, forest and agricultural wastes) in the northern hemisphere from November to March and in the southern hemisphere from May to October. The dynamic processes allow

redistribution of such emissions on a more global scale. During TRACE-A campaign, plumes loaded with high O<sub>3</sub> over the Atlantic were attributed to biomass burning emissions from Africa [7]. More recently high CO mixing ratios over Indian Ocean have been attributed to African biomass burning [8].

Surface ozone concentration may rise by up to 50 ppbv during the biomass burning seasons. Biogenic emissions yield between 5 and 30 ppbv increase in the near surface ozone concentration over tropical Africa. The impact of lightning on surface ozone is negligible. Anthropogenic emissions yield a maximum of 7 ppbv increase in the annual-mean surface ozone concentration over Nigeria, South Africa and Egypt [9].

As explained earlier, ozone in the boundary layer is a pollutant. The health impact of ozone depends on the age group and health status of individuals. The current WHO air quality guidelines in the year 2000 for O<sub>3</sub> provide a guideline value of 120 µg/m<sup>3</sup> (60 ppb), based on controlled human exposure studies, for a maximum 8-h concentration [10]. European emissions cause 50–150 additional violations per year in northern Africa and in the Near East estimated 19,000 additional mortalities occur from exposure to European ozone pollution and 50,000 additional deaths globally; the majority of the additional deaths occurs outside of Europe [11].

Regener [12] and Junge [13] consider the stratosphere to be the main source from which ozone enters the troposphere via tropopause exchange processes. Ozone is transported from the lower stratosphere into the upper troposphere through tropopause folding [14, 15] and is exchanged with the troposphere via diabatic processes and turbulent diffusion [16], mixing processes and convective erosion during the breakup of stratospheric filaments [17, 18].

Thunderstorms inject NO<sub>x</sub> mainly into the relatively clean upper troposphere. Measurements of O<sub>3</sub> in clouds indicate that both production and loss mechanisms exist. Locally within the cloud the concentrated nitrogen oxide (NO) reacts with ambient O<sub>3</sub> to produce nitrogen dioxide (NO<sub>2</sub>) which reduces the O<sub>3</sub> abundance accordingly. Lightning NO<sub>x</sub> is also responsible for a large fraction of the O<sub>3</sub> produced in the troposphere [19].

Dickerson *et al.* [20] measured enhanced mixing ratios inside a cloud compared with the boundary layer value; Poulida *et al.* [21] measured high O<sub>3</sub> near but not within a thunderstorm anvil. Both attributed this effect to intrusion of stratospheric air. Hauf *et al.* [22] detected a drop in O<sub>3</sub> on entering the anvil core of a thunderstorm cloud. Similar measurements by Ridley *et al.* [23] and Huntrieser *et al.* [24] also showed no systematic increase of in-cloud O<sub>3</sub> concentrations. By contrast, Drapcho *et al.* [25] found a correlation between a decrease in O<sub>3</sub> and an increase in NO<sub>2</sub> caused by the production of NO, followed by its reaction with O<sub>3</sub>. Recent laboratory studies of arc discharges also indicate a large ratio of NO/NO<sub>2</sub> and minimal O<sub>3</sub> production [26]. According to Price and colleagues [27, 28], equatorial Africa is one of lightning hot spot regions of the world. Marufu *et al.* [29] showed that 27% of the troposphere O<sub>3</sub> abundance observed over Africa is caused by lightning induced nitrogen oxides (LNO<sub>x</sub>).

During the MOZAIC flight over equatorial Africa, on few occasions of several measurements, enhanced ozone and relative humidity spikes were observed. The main focus of this work is to investigate the causes and sources for the enhancements. These enhancements are spikes, covering very small region and dispersed. Different data sources such as potential vorticity, ozone records of GOME from ECMWF ERA-interim and proxy parameters for convection, latent heat, outgoing long wave radiation (OLR), vertical wind and zonal (U) and meridional (V) fields were used for diagnosis of the event. This work also discusses how these events influence the ozone distribution over the equatorial troposphere. The paper is structured as follows. In Section 2, the data and methodology used in this work will be presented. Section 3 gives a brief description of both MOZAIC ozone and relative humidity spike observations. Section 4 is devoted to the result and discussion. Finally, conclusion will be presented in Section 5.

## 2 DATA AND METHODOLOGY

Measurements of ozone in the MOZAIC program are taken every four seconds from take-off to landing. Based on the dual-beam UV absorption principle (Model 49-103 from Thermo Environment Instruments, USA), the ozone measurement accuracy is estimated to be  $\pm[2 \text{ ppbv} + 2\%]$  [30]. From the beginning of the program in 1994, the measurement quality control procedures have remained unchanged to ensure long-term series are free of instrumental artifacts. Instruments are laboratory calibrated before and after the flight periods, the duration of which is generally 12–18 months. The laboratory calibration is performed with a reference analyzer which is periodically cross checked at the National Institute of Standards and Technology in France. Additionally during the flight operation period, the zero and the calibration factor of each instrument are regularly checked using a built-in ozone generator. Furthermore, comparisons are made between aircraft when they fly close in location and time, which happen several times a month. Ozone measurements from the MOZAIC program were validated by comparisons with the ozone sounding network [31]. Data are recorded from aircraft take-off to landing, providing vertical profiles and cruise data between 8 and 12.5 km altitude.

In this study, only cruise data between 20 S and 20 N were considered. In addition to MOZAIC data records, additional data such as potential vorticity,  $\text{O}_3$  VMR, cloud liquid water content, vertical, zonal and meridional wind fields derived from ECMWF ERA-interim were used. The data sets are with variable vertical resolution in pressure level with a 6-hourly analysis frequency, i.e. 0, 06, 12 and 18 UTC. For this work, data sets at 12 and 18 UTC were used. The vertical levels used for this analysis were partitioned in such a way that there are 6 levels within 900–775 hPa layer at an interval of 25 hPa, 11 levels within 750–250 hPa layer at an interval of 50 hPa, 7 levels within 250–100 hPa layer at interval of 25 hPa, 2 levels at 70 and 50 hPa each. Pressure on isentropic surface at 370, 395, 430 and 475 K were overlaid on the PV plot to distinguish the modes of airmass transport. The ERA-interim data sets are given on a horizontal resolution of  $1.5 \times 1.5$ .

The ERA-Interim data assimilation has T255 horizontal resolution, better formulation of background error constraint, reprocessed ozone profiles from GOME data from the Rutherford Appleton Laboratory from 1995 onwards and CHAMP GPS radio occultation measurements, reprocessed by university corporation for atmospheric research (UCAR). ERA-Interim uses mostly the sets of observations acquired for ERA-40, supplemented by data for later years from ECMWF's operational archive. EUMETSAT provided reprocessed winds and clear-sky radiances from Meteosat-2 (1982–1988) for ERA-40 and has reprocessed later Meteosat data for ERA-Interim [32].

The latent heat data set was retrieved from Mirador, Goddard earth sciences data and information center. Mirador contains a series of land surface parameters simulated from the Common Land Model (CLM) V2.0 model in the Global Land Data Assimilation System (GLDAS). The data are in 1.0 degree resolution and range from 1979 to the present. The temporal resolution is 3 h [33].

OLR was used to investigate the convective phenomena. NOAA daily mean Interpolated OLR data from NCAR archives, with gaps filled with temporal and spatial interpolation 2.5 degree latitude  $\times$  2.5 degree longitude global grid ( $144 \times 73$ ) [34].

The pressure and temperature profiles used to identify tropopause level were obtained from NASA Goddard Space Flight Center's Laboratory for Atmospheres. The tropopause level was calculated using the methodology proposed by Hughes. The major premise upon which the numerical method rests is the WMO operational definition for tropopause [35].

## 3 MOZAIC OZONE AND RELATIVE HUMIDITY OBSERVATION

Tropospheric ozone is a trace gas with a large natural variability in space and time and a mixing ratio in the range of about 10–100 ppbv [36].  $\text{O}_3$  volume mixing ratio of exceeding 100 ppbv were

observed in very few MOZAIC flights during 1995–1997 over the equatorial Africa region (10 S–10 N) within 250–200 hPa baro-altitude range. Four of the spiky ozone and relative humidity enhancements listed in Table 1 are depicted in Fig. 1. There are only two possibilities for the observed ozone enhancements: in situ production or vertical transport during stratospheric intrusion. In situ chemical production in the troposphere cannot lead to O<sub>3</sub> VMRs of 150–300 ppbv. This pathway is disregarded right from the outset of the analysis. The other possible source of O<sub>3</sub> rich air masses are stratospheric intrusion. High relative humidity (>100%) also observed at this cruise level over the region of elevated O<sub>3</sub> VMR. The release of latent heat affects the lapse rate, which is the rate at which atmospheric temperature declines with height. An ascending parcel of air cools as it expands. Parcels increase their RH rapidly as they ascend, Dessler and Sherwood [37] in their work on upper tropospheric humidity, reported RH = 20% at 300 hPa will saturate (RH = 100%) at about 215 hPa.

Since the relative humidity content of the stratosphere is very low, less than 50% [36], in addition to stratospheric intrusion there has to be other physical process happening in the troposphere. Thunderstorm activity would be one of the most likely events that could produce high latent heat and hence relative humidity record in the order of 100% in the vicinity of high ozone observation (see Fig. 1). Table 1 summarizes the mean enhanced ozone and relative humidity observations.

We investigated the presence of the coupled events, intrusion and convection; first, we have investigated the existence of ozone transport across the tropopause during intrusion. Potential vorticity was used to investigate stratospheric intrusion which induces very high ozone VMR to the troposphere. Vertical velocity, OLR, cloud liquid water content and latent heat flux data set of the same day were used to see convective activity that could lead to the transport of cloud liquid water content to the upper troposphere where the airplane measure high relative humidity.

#### 4 RESULTS AND DISCUSSION

To address the premises outlined above, first, we investigated the existence of stratospheric intrusion at the area of the flight prior to the plane traversing the route. The selected four events occurred before mid night that is on May 4, 1995 at 21:15:58–22:19:59 UTC, at 21:38:32–21:47:16 UTC on February 27, 1996, at 21:16:31–21:12:39 UTC on March 27, 1997 and after mid night at 04:02:58–04:07:02 UTC on April 19, 1997. Therefore, we used potential vorticity ahead of the events at 18 UTC.

Table 1: Enhanced ozone and relative humidity spikes observation at equatorial Africa at a flying altitude of 250–200 hPa.

Date	Time (UTC)	Observation site		Mean ozone (ppbv)	Mean relative humidity, humidity (%)
		Latitude (deg)	Longitude (deg)		
95.05.04	21:15:58–22:19:59	5.34–6.02	29.71–29.75	109.98	114.65
96.02.21	21:16:31–21:12:39	–6.67–7.16	26.90–27.03	124.8	180.08
96.02.27	22:10:59–22:15:59	5.34–6.02	29.71–29.75	99.66	126.95
96.05.30	21:13:50–21:17:14	1.17–1.62	29.36	109.61	87.80
97.01.18	01:33:04–01:49:03	0.22–0.67	24.66–24.79	111.76	142.19
97.03.27	22:20:30–22:24:54	1.69–2.26	25.80–25.87	135.10	134.95
97.04.19	04:02:58–04:07:02	1.21–1.46	24.34–24.78	154.56	103.44
97.04.24	03:25:51–03:29:03	4.91–5.66	23.82–24.04	182.89	153.26

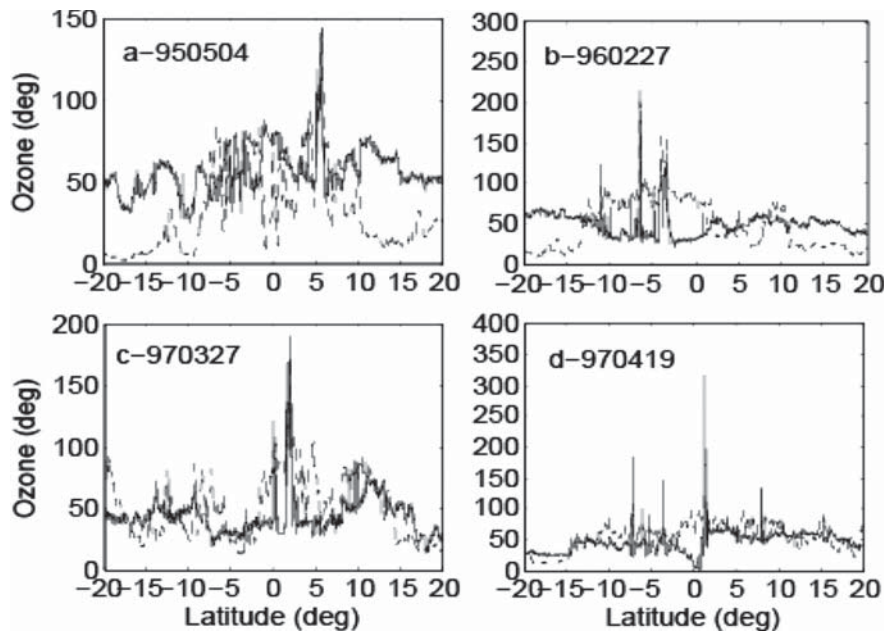


Figure 1: MOZAIC cruise ozone (solid line) and relative humidity (dash line) spikes observed on 04 May 1995, 27 February 1996, 27 March and 19 April 1997 at the flying altitude of 250–200 hPa.

Figure 2 shows ozone VMR overlaid by wind fields (upper panels) plotted below the tropopause at 100 hPa (the first ECMWF-data level below the tropopause) and daily mean OLR (lower panels). There is a clear relationship between OLR ( $<220 \text{ w/m}^2$ ) and convection as revealed by the overlaid wind fields in the upper panels of Fig. 2. In particular, the relationship is more apparent over regions surrounding locations  $5^\circ \text{ S}$ ,  $20^\circ \text{ E}$  on May 4, 1995,  $10^\circ \text{ S}$ ,  $40^\circ \text{ E}$  and  $10^\circ \text{ N}$ ,  $25^\circ \text{ E}$  on February 27, 1996; and covering regions enclosed by  $20^\circ\text{--}30^\circ \text{ E}$ ,  $10^\circ\text{--}20^\circ \text{ S}$  as well as  $0^\circ\text{--}10^\circ \text{ N}$ ,  $20^\circ \text{ W}$  on April 18, 1997. Very high ozone VMR is observed in the regions of low OLR and the overlaid stream lines showed anticyclonic curvature in all cases over ozone rich region with the exception of panel c of Fig. 2 indicating there were upper-level outflows. However, in panel c of Fig. 2, there is cyclonic curvature south of peak ozone axis and anticyclonic curvature on its northern side which likely indicates descending motion on its southern side and ascending motion over the northern side of peak ozone axis.

The latitudinal cross-section potential vorticity for the 4 days at 18 UTC are depicted in Fig. 3. The cross sections were made at the region of high ozone VMR observations at  $25.5^\circ \text{ E}$  and  $37.5^\circ \text{ E}$  for March 27 and April 18, 1997, respectively. For May 4, 1995 and February 27, 1996 the longitudinal cross section was made at  $15^\circ \text{ E}$  and  $25.5^\circ \text{ E}$  across strong convective events. High potential vorticity value greater than 2 PVU is well below tropopause level (marked by black crosses) determined using numerical model based on WMO operational definition of tropopause [35]. In addition, PV tongues cross the isentropic surfaces indicated by white dotted lines overlaid on the PV plots. These cases demonstrate the existence of stratospheric intrusion. Stratospheric intrusions are capable of inducing high concentration ozone of stratospheric origin to the troposphere. Comparing the

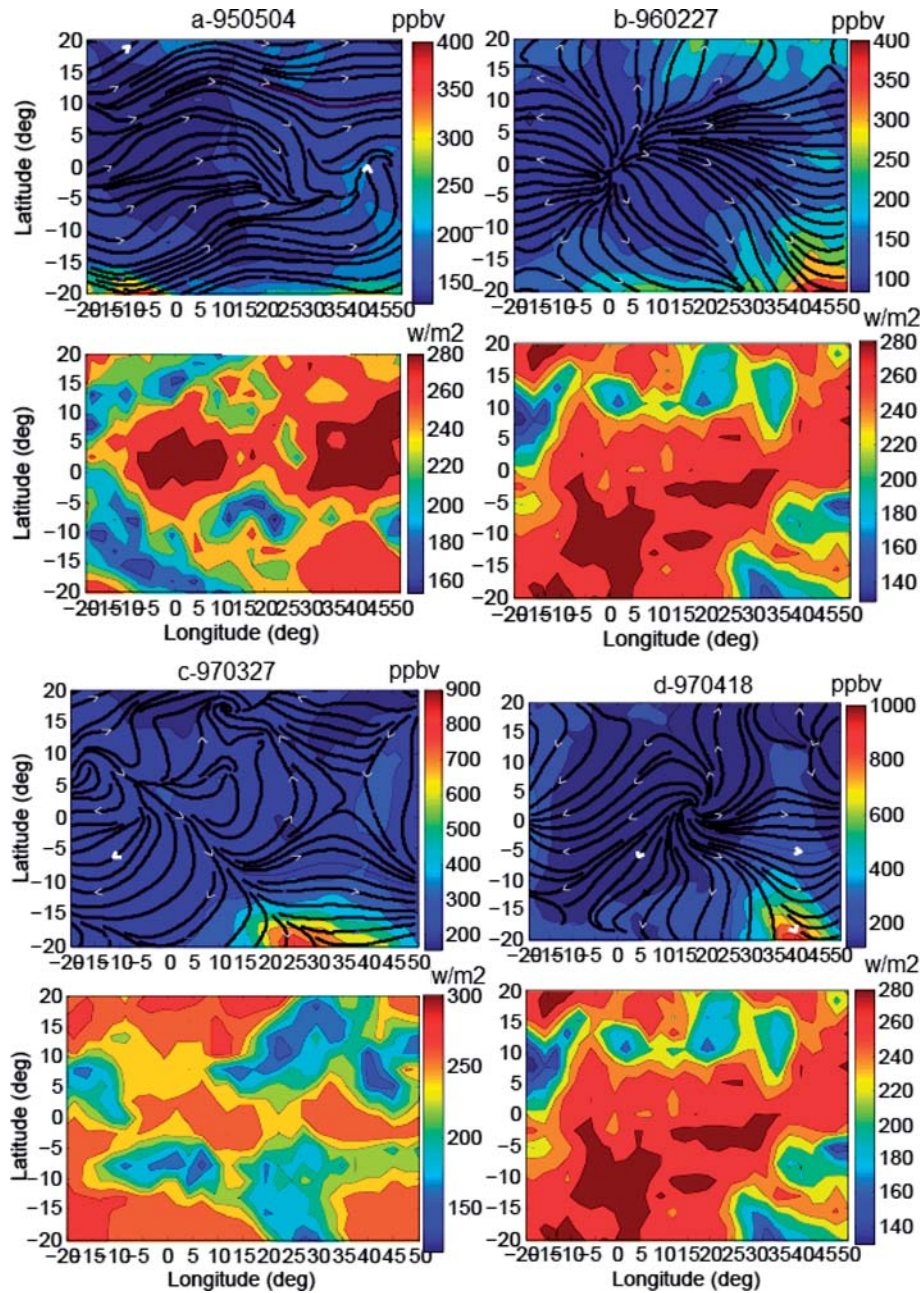


Figure 2: Ozone distributions at 100 hPa level (upper panels) and OLR (lower panels) for May 4, 1995 (a), February 27, 1996 (b), March 27, 1997 (c) and April 18, 1997 (d) at 18 UTC. The black lines overlaid on the ozone plots are wind fields.

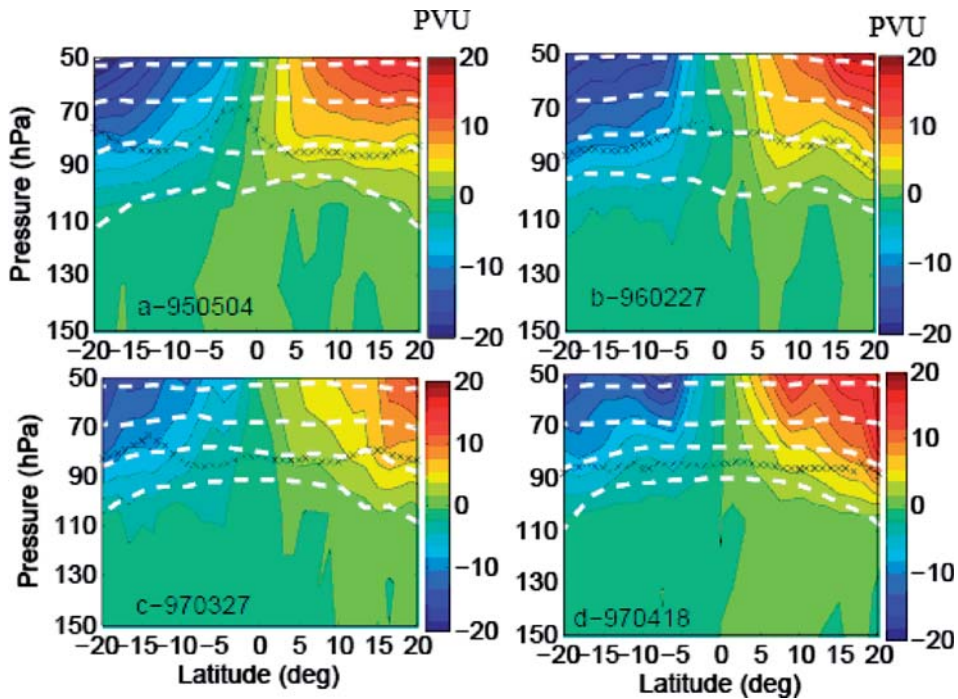


Figure 3: Potential vorticity vertical cross section at 25.5° E for May 4, 1995 (a), at 15° E for February 27, 1996 (b), at 25.5° E for March 27, 1997 (c), at 37.5° E for April 18, 1997 (d) at 18 UTC. Black cross lines show the tropopause levels and the white dashed lines represent isentropic levels at 370, 395, 430 and 475 K.

high ozone VMR in southern hemisphere 10°–20° S shown in Fig. 2c, d and PV depicted in Fig. 3c, d illustrates the relationship between ozone and potential vorticity.

The meridional cross-section of ozone mass mixing ratio profile is shown in Fig. 4 (for clarity the altitude is restricted to 1000–100 hPa layer). In all observations, enhanced ozone concentration of about 240 ppbv is observed at 100 hPa. Ozone descends down with a decreasing concentration all the way down towards the boundary layer. At the boundary layer 0–2 km (surface to 780 hPa), where ozone is considered as a pollutant, enhanced ozone is observed.

The upper panels for May 4, 1995 and for February 27, 1996 are cross-sectioned across the convective regions. Both figures illustrate how intrusion and convective events are strongly affecting the vertical ozone distribution. Convection is likely to deplete the ozone distribution 900–600 hPa on May 4, 1995 and between 900–600 hPa and 400–200 hPa on February 27, 1996. The lower panels of Fig. 4 for March 27, 1997 and April 18, 1997 show the highest ozone VMR in the regions of highest PV intrusion. In both cases, the high PV penetration able to transport very high ozone concentration of the order of 1000 ppbv as can be seen on the lower panels of Fig. 2. The strong PV intrusion able to transport very high ozone up to 100–400 hPa, the atmospheric up and down welling action further transport it up to 900 hPa levels. Ozone VMR of 60 ppbv was recorded on March 27, 1997 and up to 100 ppbv on April 18, 1997 at 900 hPa. This ozone VMR at the levels indicated could produce ozone pollution.

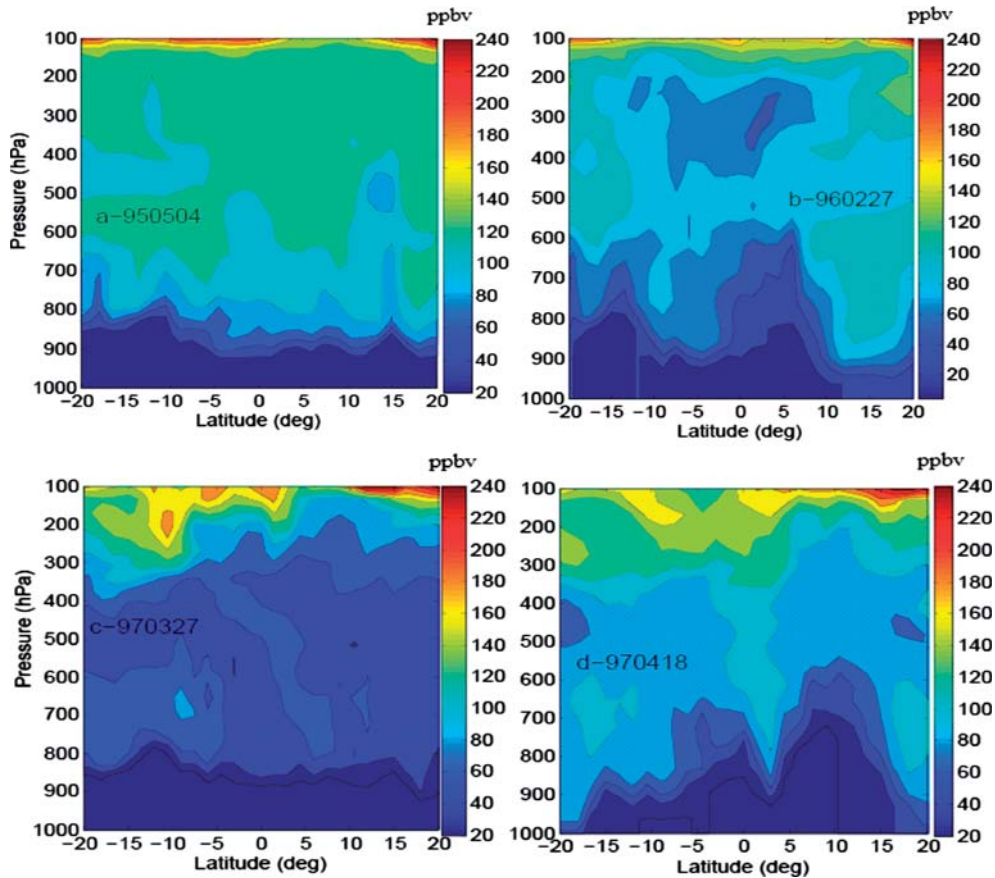


Figure 4: Ozone VMR vertical cross section at  $25.5^{\circ}$  E for May 4, 1995 (a), at  $15^{\circ}$  E for February 27, 1996 (b), at  $25.5^{\circ}$  E for March 27, 1997 (c) and at  $37.5^{\circ}$  E for April 18, 1997 (d) at 18 UTC.

In addition to OLR and wind fields discussed in Fig. 2, the existence of convective air movement was confirmed using vertical wind ( $\omega$ ) and latent heat. Large amount of latent heat is released during thunderstorm. Latent heat released in deep convective tropics, is a very important source of energy for the general circulation of the atmosphere [38]. According to Kiladis [39], the upper-level PV initiates and supports convection by destabilizing the lower troposphere and causing upward motion ahead of the tongues. The existing hypothesis for connection between PV intrusions and convection proposes that convection occurs as a result of decreased static stability and enhanced upward motion in the area of positive vorticity advection ahead of the intrusion [39]. The intrusions transport high-ozone, low-water vapor stratospheric air into the subtropical middle–upper troposphere while the convection ahead of the intrusion transport low-ozone, high-water vapor air into the upper troposphere [40]. There is strong vertical air mass transport in the regions of low OLR (threshold  $205 \text{ Wm}^{-2}$ , e.g. Gettelman and de F. Forster [41]).

Since no lightning data available during this time, we have used additional proxy parameters such as cloud liquid water content and latent heat data which are indicators of the existence of thunderstorm activity. Thunderstorm is associated with release of very high latent heat. On February 27, 1996,

very strong latent heat in the region of cloud cover was observed. For instance, at  $15.5^{\circ}$  S, the latent heat records at 09, 12, 15 and 18 UTC were 281, 534, 469,  $164.5 \text{ W/m}^2$ , respectively (see Fig. 5 left panel). Again for the April 18, 1997, the latent heat flux at 09, 12, 15 and 18 UTC at  $12.5^{\circ}$  S are 188, 431, 188,  $6.9 \text{ W/m}^2$ . From these records, it is apparent that thunderstorm dissipation likely to occur between 12 and 15 UTC because the heat flux grew from 09 to 12 UTC and then decreased in between 12 and 15 UTC. In addition, cloud liquid water transport is another indicator of thunderstorm activity. Comparison of cloud liquid water content between 12 and 18 UTC of each day (Fig. 6a, b for February 27, 1996 and Fig. 6c, d for April 27, 1997) shows a spatial variability with time. This observation reveals a clear transport of liquid water content that is the main manifestation of the existence of thunderstorm in the vicinity of pick latent heat observations. The liquid water content may be transported further upward to upper troposphere where the air plane records high relative humidity between 21 and 04 UTC.

Vertical wind ( $\omega$ ) further demonstrates the existence of convective activity at  $5^{\circ}$ – $10^{\circ}$  N from 1000 to 600 hPa and  $5^{\circ}$  S– $5^{\circ}$  N 200–400 hPa and  $15^{\circ}$  S on February 27, 1996 (see Fig. 7 left panel). In the localities indicated ozone VMR is depleted due to convective erosion (see Fig. 4b). Similar case is shown in Fig. 7b where there is convection at 1000–700 hPa around  $0^{\circ}$  latitude, 900–500 hPa at about  $5^{\circ}$ – $15^{\circ}$  N, downward air movement from 900 to 450 hPa mainly between  $0^{\circ}$  and  $5^{\circ}$  N for the April 18, 1997. These two cases clearly show how ozone distribution affected by vertical wind field.

The above discussions show how ozone of stratospheric origin transported during PV intrusion and the effect of convection on the distribution of ozone. The two main factors that deplete the ozone concentration are thunderstorm and convective erosion. During thunderstorm the high voltage causes dissociation in the oxygen molecules to atomic oxygen then further reaction of oxygen atom with oxygen molecule produces ozone. Ozone produced by this mechanism is very low. The lightning event also favors high NO production. NO reacts with ozone which leads to the production of  $\text{NO}_2$  which is manifested in a decrease of  $\text{O}_3$  concentration. The net result is reduction of ozone or scavenging within the thunderstorm cloud. According to Hill *et al.* [42] and Franzblau [43].  $\text{NO}_x$  ( $\text{NO} + \text{NO}_2$ ) is produced mainly by hot lightning strokes, in contrast ozone may be destroyed in hot flash channel [44]. Vertical wind field triggered by latent heat and PV intrusion reduces ozone concentration. These events produce convective erosion.

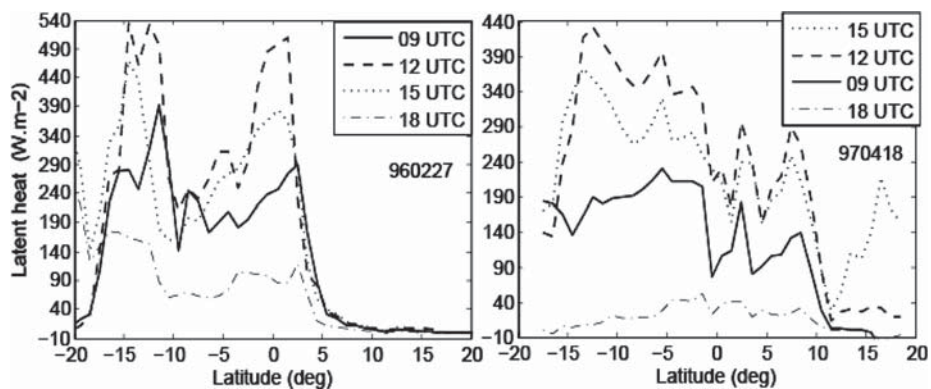


Figure 5: Latent heat at  $25.5^{\circ}$  E for February 27, 1996 (left panel) and  $37.5^{\circ}$  E for April 18, 1997 (right panel).

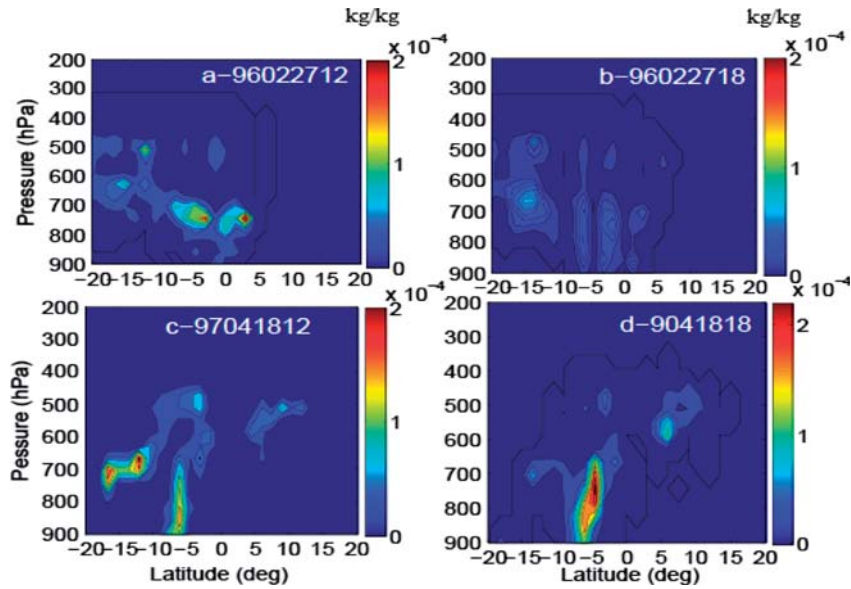


Figure 6: Meridional cross-section of liquid water content transport between 12 and 18 UTC at 15° E for February 27, 1996 (upper panel) and at 37.5° E for April 18, 1997 (lower panel).

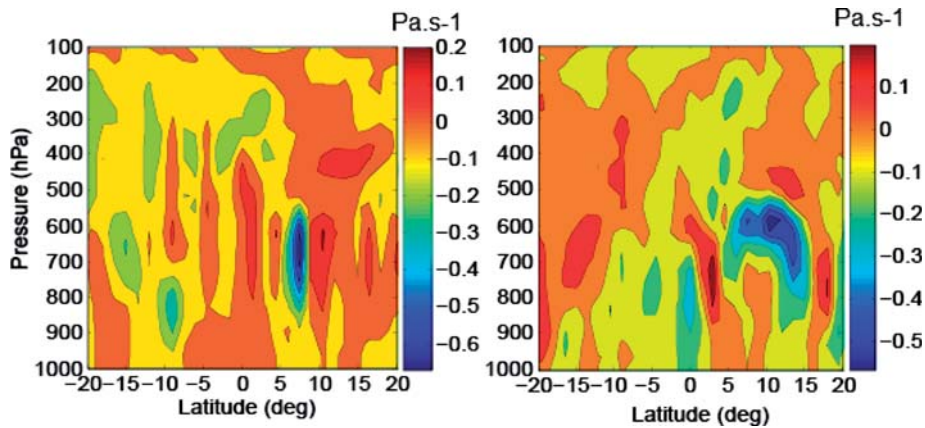


Figure 7: Meridional cross-section of vertical wind field ( $\omega$ ) at 15° S for February 27, 1996 (left panel) and 37.5° E for April 18, 1997 (right panel).

## 5 CONCLUSIONS

In this work, enhanced MOZAIC ozone and relative humidity spikes exceeding 100 ppbv and 100%, respectively, observed over equatorial Africa have been analyzed. Stratospheric intrusion coupled to convection found to be the key physical process that attributed to spiky O<sub>3</sub> VMR and relative humidity observations. Potential vorticity values exceeding 2 PVU observed below the tropopause level confirms stratospheric intrusion.

Convection was investigated using proxy parameters. The vertical wind field ( $\omega$ ), low daily mean OLR value (<220 W/m<sup>2</sup>) and very high latent heat indicate the presence of deep convection. Very high latent heat release and cloud liquid water transport indicate the existence of thunderstorm activity over the area of deep convective regions.

Using ECMWF ERA-interim ozone VMR, the possible ozone distribution within the troposphere during these two dynamical events was observed. Very low ozone of the order about 20 ppbv within the deep convective regions was observed. Convective erosion is the main mechanism that depletes ozone mainly at the boundary layer. Low ozone VMR observed within the thunderstorm cloud is in agreement with previous reports. Very high ozone of stratospheric origin (>200 ppbv) introduced during PV intrusion to upper equatorial troposphere. The intruding stratospheric ozone was able to make its way down to boundary layer. These processes have resulted in ambient air pollution with O<sub>3</sub> VMR exceeding the proposed WHO guideline limit of 60 ppbv.

## REFERENCES

- [1] Prather, M. & Ehhalt, D., Atmospheric chemistry and greenhouse gases. *Climate Change the Scientific Bases*, eds J.T. Houghton *et al.*, Cambridge University Press: Cambridge, 2001.
- [2] Marufu, L., Dentener, F., Lelieveld, J., Andreae, M. & Helas, G., Photochemistry of the African troposphere: influence of biomass-burning emissions. *J. Geophys. Res.*, **105**, pp. 14 513–14 530, 2000.
- [3] Jaegl'e, L., Steinberger, L., Martin, R. & Chance, K., Global partitioning of NO<sub>x</sub> sources using satellite observations: relative roles of fossil fuel combustion, biomass burning and soil emissions. *Faraday Discuss*, **130**, pp. 407–423, 2005.
- [4] Schumann, U. & Huntrieser, H., The global lightning induced nitrogen oxides source. *Atmos. Chem. Phys.*, **7**, pp. 3823–3907, 2007. doi:<http://dx.doi.org/10.5194/acp-7-3823-2007>
- [5] Jonqui`eres, I., Marenco, A., Maalej, A. & Rohrer, F., Study of ozone formation and transatlantic transport from biomass burning emissions over West Africa during the airborne tropospheric. Ozone campaigns TROPOZ I and TROPOZ II. *J. Geophys. Res.*, **103**, pp. 19 059–19 074, 1998.
- [6] Andreae, M.O., The influence of tropical biomass burning on climate and the atmospheric environment. *Biogeochemistry of Global Change: Radiatively Active Trace Gases*, ed. R.S. Oremland, Chapman and Hall: New York, pp. 113–150, 1993.
- [7] Singh, H.B., Herlth, D. & Koyler, R., Impact of biomass burning emissions on the composition of the South Atlantic troposphere: reactive nitrogen and ozone. *J. Geophys. Res.*, **101**, pp. 24 203–24 220, 1996.
- [8] Edwards, D.P. e. a., Satellite-observed pollution from southern hemisphere biomass burning. *J. Geophys. Res.*, **111**, doi:10.1029/2005JD006 655, 2006. doi:<http://dx.doi.org/10.1029/2005JD006>
- [9] Aghedo, A.M., Schultz, M.G. & Rast, S., The influence of African air pollution on regional and global tropospheric ozone. *Atmos. Chem. Phys.*, **7**, pp. 1193–1212, 2007. doi:<http://dx.doi.org/10.5194/acp-7-1193-2007>

- [10] Report on a WHO Working Group, *Health Aspects of Air Pollution with Particulate Matter, Ozone and Nitrogen Dioxide*. Bonn, Germany, 13–15, 2003.
- [11] Duncan, B.N., West, J.J., Yoshida, Y.A., Fiore, M. & Ziemke, J.R., The influence of European pollution on ozone in the Near East and northern Africa. *Atmos. Chem. Phys. Discuss.*, **8**, pp. 1913–1950, 2008. [doi:http://dx.doi.org/10.5194/acpd-8-1913-2008](http://dx.doi.org/10.5194/acpd-8-1913-2008)
- [12] Regener, V.H., Vertical flux of atmospheric ozone. *J. Geophys. Res.*, **62**, pp. 221–228, 1957. [doi:http://dx.doi.org/10.1029/JZ062i002p00221](http://dx.doi.org/10.1029/JZ062i002p00221)
- [13] Junge, C.E., Global ozone budget and exchange between stratosphere and troposphere. *Tellus*, **14**, pp. 363–377, 1962. [doi:http://dx.doi.org/10.1111/j.2153-3490.1962.tb01349.x](http://dx.doi.org/10.1111/j.2153-3490.1962.tb01349.x)
- [14] Danielsen, E.F., Stratospheric-tropospheric exchange based on radioactivity, ozone and potential vorticity. *J. Atmos. Sci.*, **25**, pp. 502–528, 1968. [doi:http://dx.doi.org/10.1175/1520-0469\(1968\)025<0502:STEBOR>2.0.CO;2](http://dx.doi.org/10.1175/1520-0469(1968)025<0502:STEBOR>2.0.CO;2)
- [15] Danielsen, E.F., Hiskind, R.S., Gaines, S.E., Sachse, G.W., Gregory, G.L. & Hill, G.F., Three-dimensional analysis of potential vorticity associated with tropopause folds and observed variations of ozone and carbon monoxide. *J. Geophys. Res.*, **92**, pp. 2103–2111, 1987. [doi:http://dx.doi.org/10.1029/JD092iD02p02103](http://dx.doi.org/10.1029/JD092iD02p02103)
- [16] Lamarque, J.F. & Hess, P.G., Cross-tropopause mass exchange and potential vorticity budget in a simulated tropopause folding. *J. Atmos. Sci.*, **51**, pp. 2246–2269, 1994. [doi:http://dx.doi.org/10.1175/1520-0469\(1994\)051<2246:CTMEAP>2.0.CO;2](http://dx.doi.org/10.1175/1520-0469(1994)051<2246:CTMEAP>2.0.CO;2)
- [17] Appenzeller, C., Holton, J.R. & Rosenlof, K.H., Seasonal variation of mass transport across the tropopause. *J. Geophys. Res.*, **101(D10)**, pp. 15071–15078, 1996. [doi:http://dx.doi.org/10.1029/96JD00821](http://dx.doi.org/10.1029/96JD00821)
- [18] Gouget, H., Vaughan, G., Marengo, A. & Smit, H.G.J., Decay of a cut-off low and contribution stratosphere-troposphere exchange. *Q. J. R. Meteorol. Soc.*, **126**, pp. 1117–1141, 2000. [doi:http://dx.doi.org/10.1256/smsqj.56413](http://dx.doi.org/10.1256/smsqj.56413)
- [19] Grewe, V., Impact of climate variability on tropospheric ozone. *Sci. Total Environ.*, **374**, pp. 167–181, 2007. [doi:http://dx.doi.org/10.1016/j.scitotenv.2007.01.032](http://dx.doi.org/10.1016/j.scitotenv.2007.01.032)
- [20] Dickerson, R.R. *et al.*, Thunderstorms: an important mechanism in the transport of air pollutants. *Science*, **235**, pp. 460–464, 1987. [doi:http://dx.doi.org/10.1126/science.235.4787.460](http://dx.doi.org/10.1126/science.235.4787.460)
- [21] Poulida, O. *et al.*, Stratosphere-troposphere exchange in a midlatitude mesoscale convective complex observations. *J. Geophys. Res.*, **101(D3)**, pp. 6823–6836, 1996. [doi:http://dx.doi.org/10.1029/95JD03523](http://dx.doi.org/10.1029/95JD03523)
- [22] Hauf, T. *et al.*, Rapid vertical traces gas transport by an isolated multitude thunderstorm. *J. Geophys. Res.*, **100(D11)**, pp. 22957–22970, 1995. [doi:http://dx.doi.org/10.1029/95JD02324](http://dx.doi.org/10.1029/95JD02324)
- [23] Ridley, B.A. *et al.*, Distribution of NO, NO<sub>x</sub>, NO<sub>y</sub>, and O<sub>3</sub> at 12 km altitude during the summer monsoon season over New Mexico. *J. Geophys. Res.*, **99(D12)**, pp. 25519–25534, 1994. [doi:http://dx.doi.org/10.1029/94JD02210](http://dx.doi.org/10.1029/94JD02210) [doi:http://dx.doi.org/10.1029/94JD02210](http://dx.doi.org/10.1029/94JD02210)
- [24] Huntrieser, H. *et al.*, Transport and production of NO<sub>x</sub> in electrified thunderstorms: survey of previous studies and new observations at midlatitudes. *J. Geophys. Res.*, **103(21)**, pp. 28247–28264, 1998. [doi:http://dx.doi.org/10.1029/98JD02353](http://dx.doi.org/10.1029/98JD02353)
- [25] Drapcho, D.L. *et al.*, Nitrogen fixation by lightning activity in a thunderstorm. *Atmos. Environ.*, **17(4)**, pp. 729–734, 1983.
- [26] Wang, Y. *et al.*, Nitric oxide production by simulated lightning: dependence on current, energy, and pressure. *J. Geophys. Res.*, **103(D15)**, pp. 19149–19159, 1998. [doi:http://dx.doi.org/10.1029/98JD01356](http://dx.doi.org/10.1029/98JD01356)
- [27] Price, C., Lightning sensors for observing, tracking and now casting severe weather. *Sensors*, **8**, pp. 157–170, 2008. [doi:http://dx.doi.org/10.3390/s8010157](http://dx.doi.org/10.3390/s8010157)

- [28] Price, C. & Asfur, M., Can lightning observations be used as an indicator of upper-tropospheric water vapor variability? *American Meteorological Society*, **87(3)**, pp. 291–298, 2006. [doi:http://dx.doi.org/10.1175/BAMS-87-3-291](http://dx.doi.org/10.1175/BAMS-87-3-291)
- [29] Marufu, L., Dentener, F., Lelieveld, J., Andreae, M.O. & Helas, G., Photochemistry of the African troposphere: influence of biomass-burning emissions. *J. Geophys. Res.*, **105(2248)**, pp. 14513–14530, 2000. [doi:http://dx.doi.org/10.1029/1999JD901055](http://dx.doi.org/10.1029/1999JD901055)
- [30] Thouret, V., Marenco, A., Nedelec, P. & Grouhel, C., Ozone climatologies at 9–12 km altitude as seen by the MOZAIC airborne program between September 1994 and August 1996. *J. Geophys. Res.*, **103(25)**, pp. 653–679, 1998.
- [31] Thouret, V., Marenco, A., Logan, J.A., Nedelec, P. & Grouhel, C., Comparisons of ozone measurements from the MOZAIC airborne program and the ozone sounding network at eight locations. *J. Geophys. Res.*, **103(25)**, pp. 695–720, 1998.
- [32] ECMWF, Website, uk: [http://wcrp.ipsl.jussieu.fr/Workshops/Reanalysis2008/Documents/V1-102\\_ea.pdf](http://wcrp.ipsl.jussieu.fr/Workshops/Reanalysis2008/Documents/V1-102_ea.pdf)
- [33] Mirador, Website: NASA Goddard, <http://mirador.gsfc.nasa.gov>
- [34] NOAA Interpolated Outgoing Longwave Radiation (OLR), website: [http://www.esrl.noaa.gov/psd/data/gridded/data.interp\\_OLR.html](http://www.esrl.noaa.gov/psd/data/gridded/data.interp_OLR.html)
- [35] Carl, M.C., *Objective Determination of the Tropopause Using WMO Operational Definitions*, U.S. Department of Commerce National Oceanic and Atmospheric Administration National Weather Service Meteorological Center, October 1981.
- [36] Zbinden, R.M., Cammas, J.P., Thouret, V., N'ed'elec, P., Karcher, F. & Simon, P., Mid-latitude tropospheric ozone columns from the MOZAIC program: climatology and interannual variability. *Atmos. Chem. Phys.*, **6**, pp. 1053–1073, 2006. [doi:http://dx.doi.org/10.5194/acp-6-1053-2006](http://dx.doi.org/10.5194/acp-6-1053-2006)
- [37] Dessler, A.E. & Sherwood, S.C., Simulation of tropical upper tropospheric humidity. *J. Geophys. Res.*, **105**, pp. 20155–20163, 2000. [doi:http://dx.doi.org/10.1029/2000JD900231](http://dx.doi.org/10.1029/2000JD900231)
- [38] Hoerling, M.P., Diabatic sources of potential vorticity in the general circulation. *J. Atmos. Sci.*, **49**, pp. 2282–2292, 1992. [doi:http://dx.doi.org/10.1175/1520-0469\(1992\)049<2282:DSOPVI>2.0.CO;2](http://dx.doi.org/10.1175/1520-0469(1992)049<2282:DSOPVI>2.0.CO;2)
- [39] Kiladis, G.N., Observations of Rossby waves linked to convection over the eastern tropical Pacific. *J. Atmos. Sci.*, **55**, pp. 321–339, 1998. [doi:http://dx.doi.org/10.1175/1520-0469\(1998\)055<0321:OORWLT>2.0.CO;2](http://dx.doi.org/10.1175/1520-0469(1998)055<0321:OORWLT>2.0.CO;2)
- [40] Waugh, D.W., Impact of potential vorticity intrusions on subtropical upper tropospheric humidity. *J. Geophys. Res.*, **110**, D11305, doi:10.1029/2004JD005664, 2005. [doi:http://dx.doi.org/10.1029/2004JD005664](http://dx.doi.org/10.1029/2004JD005664)
- [41] Gettelman, A. & de F. Forster, P.M., A climatology of the tropical tropopause layer. *Journal of the Meteorological Society of Japan*, **80(4B)**, pp. 911–924, 2002. [doi:http://dx.doi.org/10.2151/jmsj.80.911](http://dx.doi.org/10.2151/jmsj.80.911)
- [42] Hill, R.D., Rahmim, I. & Rinker, R.G., Experimental study of the production of NO, N<sub>2</sub>O, and O<sub>3</sub> in a simulated corona. *Ind. Eng. Chem. Res.*, **27**, pp. 1264–1269, 1988. [doi:http://dx.doi.org/10.1021/ie00079a029](http://dx.doi.org/10.1021/ie00079a029)
- [43] Franzblau, E., Electrical discharges involving formation of NO, NO<sub>2</sub>, HNO<sub>3</sub>, and O<sub>3</sub>. *J. Geophys. Res.*, **96**, pp. 22 337–22 345, 1991.
- [44] Noxon, J.F., Tropospheric NO<sub>2</sub>. *J. Geophys. Res.*, **83**, pp. 3051–3057, 1978. [doi:http://dx.doi.org/10.1029/JC083iC06p03051](http://dx.doi.org/10.1029/JC083iC06p03051)